

Supporting quantum technologies with an ultralow-loss silicon photonics platform

Matteo Cherchi , Arijit Bera, Antti Kemppinen, Jaani Nissilä, Kirsi Tappura , Marco Caputo, Lauri Lehtimäki, Janne Lehtinen , Joonas Govenius, Tomi Hassinen, Mika Prunnila, and Timo Aalto*

VTT Technical Research Centre of Finland Ltd., Espoo, Finland

Abstract. Photonic integrated circuits (PICs) are expected to play a significant role in the ongoing second quantum revolution, thanks to their stability and scalability. Still, major upgrades are needed for available PIC platforms to meet the demanding requirements of quantum devices. We present a review of our recent progress in upgrading an unconventional silicon photonics platform toward this goal, including ultralow propagation losses, low-fiber coupling losses, integration of superconducting elements, Faraday rotators, fast and efficient detectors, and phase modulators with low-loss and/or low-energy consumption. We show the relevance of our developments and our vision in the main applications of quantum key distribution, to achieve significantly higher key rates and large-scale deployment; and cryogenic quantum computers, to replace electrical connections to the cryostat with optical fibers.

Keywords: silicon photonics; quantum key distribution; quantum computers; cryogenic photonics; superconducting nanowire single-photon detectors; quantum technologies; superconducting qubits; silicon qubits.

Received Feb. 15, 2023; accepted for publication Feb. 22, 2023; published online Apr. 6, 2023.

© The Authors. Published by SPIE and CLP under a Creative Commons Attribution 4.0 International License. Distribution or reproduction of this work in whole or in part requires full attribution of the original publication, including its DOI.

[DOI: [10.1117/1.APN.2.2.024002](https://doi.org/10.1117/1.APN.2.2.024002)]

1 Introduction

We are presently living in the so-called second quantum revolution, where the focus has shifted from pure science to technologies and applications.¹ Photonic technologies are expected to play a major role, not only in quantum applications but also in classical configurations to support solid-state quantum systems. In particular, photonic integrated circuits (PICs) offer unique opportunities for different quantum technologies to scale up system complexity and integration density while providing unmatched performance and stability.^{2–6} In this regard, the micron-scale silicon photonics platform⁷ brings with it a unique set of properties and building blocks. This includes low propagation losses (down to 3 dB/m demonstrated to date^{8,9}), broadband and low-loss coupling to fibers (≈ 0.5 dB), fast (>40 GHz) and responsive (≈ 1 A/W) integrated germanium photodetectors,¹⁰ upreflecting mirrors (URM) for broadband and low-loss coupling to arrays of detectors, tight bends¹¹ enabling high-integration density, efficient phase shifters, low-loss Mach–Zehnder interferometers, multimillion Q ring resonators,^{9,12} polarization insensitive operation, and polarization splitters¹³ and rotators, including all-silicon Faraday rotators (FRs).¹⁴

A relevant example application is large-scale deployment of quantum key distribution (QKD), for which we are developing efficient multiplexed receivers. A second interesting case is the use of our photonic integration technology to scale up superconducting quantum computers by controlling and reading out the qubits in the cryostat through classical optical links. In this case, the major challenge is the development of suitable electrical-to-optical and optical-to-electrical converters (OECs) operating at cryogenic temperatures.

We will cover these ongoing developments as follows, showing our recent results as well as our plans to further exploit the platform. In Sec. 2, we will first give an overview of the thick-silicon photonics platform, with a special focus on the most relevant features for quantum technologies. In Secs. 3 and 4, we will cover the ongoing developments for QKD and quantum computers and then conclude in Sec. 5 and briefly mention other promising future developments and applications.

2 Overview of VTT Thick Silicon-on-Insulator Platform

We can divide the building blocks of the platform into two main categories: passives and actives. In this context, “active” means

*Address all correspondence to Timo Aalto, timo.aaalto@vtt.fi

anything requiring an electrical control, such as thermo-optic phase shifters and electro-optic modulators, or electrical readout, such as a photodiode. An overview of the main building blocks available on the platform is sketched in Fig. 1 with the notable exception of phase modulators based on PIN diodes, which are explained in detail in Sec. 2.2. We fabricate our PICs on 150-mm diameter silicon-on-insulator (SOI) wafers (to be upgraded soon to 200 mm) with 3- μm thick device layer (± 100 nm uniformity) using a UV stepper (365 nm wavelength) and a modified Bosch process^{15,16} to etch the waveguides.

2.1 Passive Building Blocks

2.1.1 Types of waveguides

The five main waveguide types available on the platform are: rib waveguides, strip waveguides, down-tapered strip waveguides, strip waveguides with a thin pedestal, and down-tapered strip waveguides with a thin pedestal (the latter is the only type missing in Fig. 1). For rib waveguides, trenches are partially etched (typically 1.2- μm deep etch) on both sides of the waveguide. Single-mode operation can be achieved for both transverse-electric (TE) and transverse-magnetic (TM) polarization with a suitable choice of the rib width¹⁷ (typically ≤ 3 μm). On the contrary, all four possible strip waveguide cross sections are inherently multimode. Nevertheless, we carefully design the optical circuits so that excitation of the higher-order modes (HOMs) is always negligible in the connecting waveguides, ensuring effective single-mode operation of the whole circuit.

2.1.2 I/O coupling

We fabricate the vertical waveguide facets of our PICs at wafer scale by first etching the silicon facet and then depositing a suitable antireflection coating, which can be made of either a single dielectric layer or multiple layers.

The coupling loss to optical fibers can be as low as 0.5 dB, provided that the mode field diameter is about 2.5 μm , which is achieved with lensed (or tapered) fibers or small core fibers with high numerical aperture. Fiber arrays must be used instead in

configurations where the PIC has several inputs and outputs. Given the limited assembly precision of fiber arrays and considering that the tolerance to misalignments scales inversely with the mode size, low-loss coupling can be ensured only by arrays of standard single-mode fibers (SMFs) with mode diameter around 10 μm . This requires suitable mode size converters, like the one shown in Fig. 2, fabricated by etching arrays of 12- μm -wide rib and strip waveguides on an SOI wafer with a 12- μm -thick device layer, and then tapering the thickness of the output strip waveguides down to 3 μm by polishing each optical interposer chip. We are presently working toward further reduction of coupling losses below 0.5 dB by implementing 3D printed lenses,¹⁸ directly printed on the waveguide facets at wafer scale. This way, we aim to couple the PIC directly to SMFs and fiber arrays with ultralow-loss and relaxed alignment tolerance¹⁹ (Fig. 3).

Light can also be coupled to the PIC vertically from URMs (see Figs. 1 and 4), which are wet etched with a negative angle. Their working principle is total internal reflection, and coupling losses are practically the same as for the vertical facets. The anti-reflection coating for URMs is the same as for vertical facets. The wet etching process occurs along crystalline planes, meaning that the mirrors can be fabricated only along the four orthogonal crystal planes with Miller indices of 110, $\bar{1}10$, $1\bar{1}0$, and $\bar{1}\bar{1}0$. One of the advantages of URMs is the possibility of using them to test the fabricated PICs at wafer scale.

Compared to grating couplers typically used in submicron waveguides, URMs support both TE and TM polarizations with negligible polarization-dependent loss, and they operate over the whole transparency range of silicon, from 1.2 to 7 μm wavelength. We additionally stress here that thick-SOI PICs can operate over the whole transparency range of silicon. In particular, one can design a rib waveguide to be single mode at all the wavelengths in that broad spectral range, spanning several octaves.¹⁷ We must emphasize that, above 3 μm wavelength, absorption in the silica cladding [including the buried oxide (BOX) and the top cladding, see Fig. 1] contributes to propagation losses. However, due to the strong confinement in the

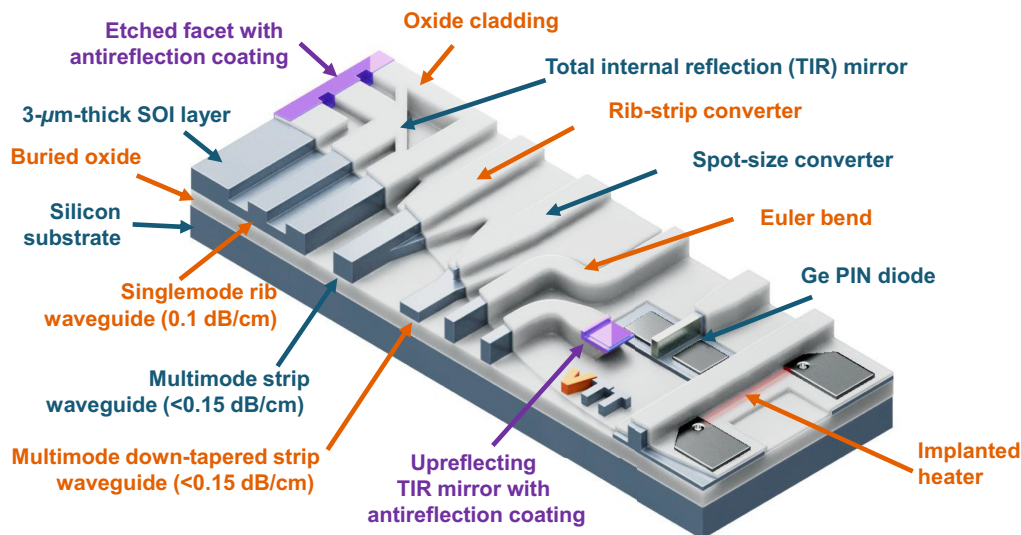


Fig. 1 Sketch of the main building blocks available on the thick-SOI platform. Typical thickness of the device layer is 3 μm , whereas the BOX thickness can vary from 400 nm to 3 μm . We define “active” building blocks as those requiring electrical pads for either control or readout.

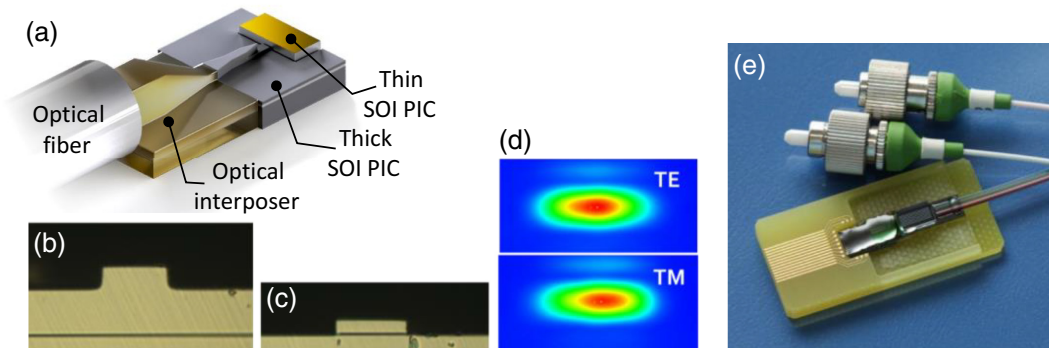


Fig. 2 (a) Sketch of different mode size conversions starting from an SMF coupled to the 3- μm thick waveguides of a thick-SOI PIC using an optical interposer fabricated on 12- μm thick SOI. The sketch also shows how the mode size can be reduced further even to couple light to submicron waveguides on a flip-chip bonded PIC that can be evanescently coupled through suitable inverse tapers. (b) Micrograph of a 12- μm thick rib waveguide of a fabricated optical interposer; (c) micrograph of a strip waveguide polished down to about 3- μm thickness on the opposite facet; (d) near-field image (infrared camera) of the TE and TM modes at the output facet of the interposer [shown in (c)]; and (e) packaged 3- μm thick-SOI PIC coupled to a fiber array through an optical interposer.

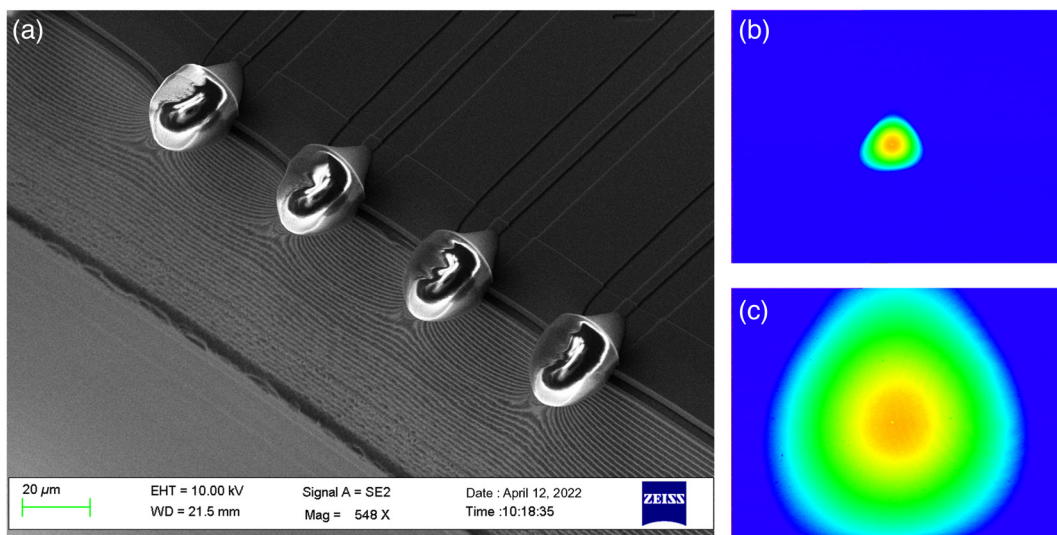


Fig. 3 (a) SEM image of polymer lenses 3D printed in front of the end facets of four rib waveguides; (b) near-field picture of the output mode of a rib waveguide taken with an infrared camera; (c) near-field picture of the output of a lensed rib waveguide [same scale as (b)].

thick silicon core, propagation losses remain below 1 dB/cm up to about 4 μm wavelength, and low propagation losses can be achieved up to 7 μm wavelength by selectively removing the silica cladding²⁰ all around the waveguide. This is in strong contrast to thin SOI-based Si photonics platforms where propagation losses are typically above 1 dB/cm even at telecom wavelengths²⁰ because of stronger interaction with the sidewall roughness. Furthermore, the power fraction in the cladding of submicron waveguide modes is orders of magnitude larger compared to thick-SOI waveguides, meaning that the absorption in the silica cladding²¹ already becomes unbearable beyond 2.5 μm wavelength. Operation in the mid-IR is critical for many gas sensing applications²²—including quantum sensing²³—and also to exploit the strong third-order nonlinearity of silicon; further,

the larger optical mode size in thick SOI enables avoiding saturation caused by strong two-photon absorption²⁴ (and associated free-carrier absorption²⁵) at wavelengths shorter than 2.2 μm . Although the large cross section of the waveguides is not ideal for efficient excitation of nonlinear effects including parasitic two-photon absorption, the unique combination with ultralow propagation losses is advantageous in many applications.^{26,27}

2.1.3 Tight bends enabling high-integration density

It is generally assumed that waveguides with micron-scale cross sections require bending radii on the order of several millimeters. This is because the index contrast ensuring single-mode operation in a micron-scale waveguide would inherently lead to

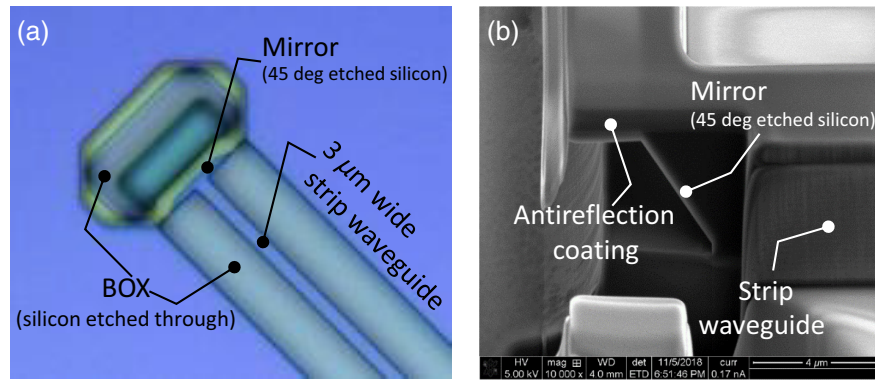


Fig. 4 (a) Micrograph of a fabricated URM and (b) side view of a vertical cross section of an URM via focused ion beam microscopy.

high radiation losses for tighter bends. In the platform, we have developed two solutions to this limitation: turning mirrors based on TIR²⁸ [Figs. 5(a) and 5(b)] and tight adiabatic bends referred to as the Euler bends [Fig. 5(a)].¹¹ The first approach applies to both rib waveguides and strip waveguides, whereas the second requires high-index contrast strip waveguides.

TIR mirrors allow for compact layouts, such as the imbalanced Mach–Zehnder interferometer (MZI) shown in Fig. 5(b), which also shows the very low-loss (≈ 0.02 dB) waveguide crossings easily achievable on the platform. Turning mirrors can be designed with almost any turning angle, and their losses can be made as low as 0.1 dB per turn using parabolic shapes and/or making the waveguide sufficiently wide. In fact, the main loss mechanism is light diffraction due to the partial lack of lateral guidance in the mirror region. Remarkably, turning mirrors work over the entire (from 1.2 to 7 μm) wavelength transparency region of silicon and can be designed to simultaneously work equally well for both TE and TM polarizations, despite the polarization-dependent offset induced by the Goos–Hänchen shift.²⁹ Nevertheless, the nonnegligible loss makes them unsuitable for circuits requiring a large number of bends, e.g., long spiral waveguides.

For this reason, we have also developed more conventional waveguide bends to achieve much lower losses. They are based on strip waveguides, ensuring negligible radiation loss due to strong light confinement. The only limitation is that they support several HOMs that get easily excited in a tight bend. We

have, therefore, introduced¹¹ and patented³⁰ a geometry with gradual a change of curvature, using the Euler spiral geometry as shown in Figs. 5(c), 6(a), and 6(b). This way, tight bends with loss lower than 0.02 dB can be achieved with effective bending radii of a few tens of microns, enabling, e.g., compact race track resonators with quality factor Q of up to 14 million.^{9,12}

Even though, in general, the wavelength range of operation of the bends is not as wide as that of turning mirrors, bends can be designed to cover bandwidths of several hundreds of nanometers up to a few microns. An interesting property of Euler bends is that they very efficiently transmit most of supported HOMs³¹ (i.e., those with effective index sufficiently higher than the cladding refractive index), as highlighted in Fig. 6(c). In other words, the bends preserve the mode power distribution, which is useful when designing PICs for mode multiplexing³² and when using spatial modes as a quantum degree of freedom^{33–36} (see also Sec. 5). It is worth mentioning that turning mirrors also preserve the HOM power distribution under reflection.³⁷

2.1.4 Polarization management

Micron-scale silicon waveguides support both TE and TM polarizations with very similar spatial mode distributions, the same propagation losses, and very similar effective indices. Indeed, strip waveguides with a square cross section can support TE and TM fundamental modes with identical propagation constants. Any possible residual birefringence induced by material

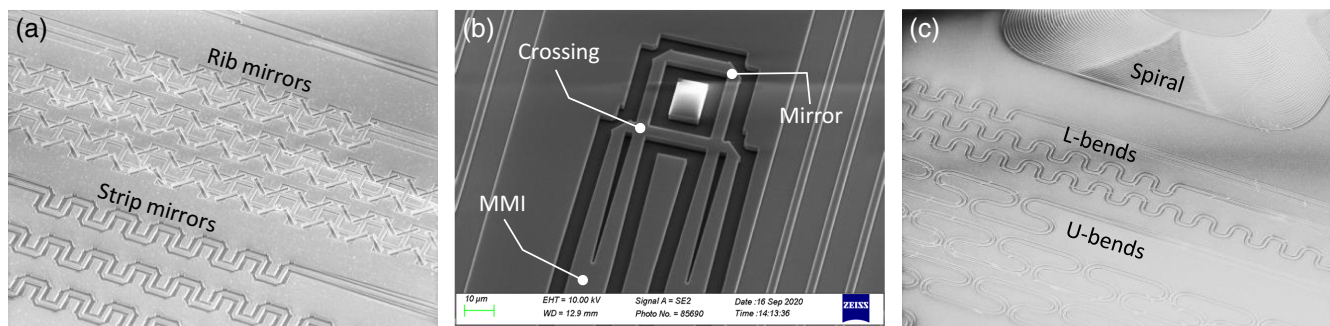


Fig. 5 (a) SEM picture of 90-degree turning mirrors on rib waveguides and strip waveguides; (b) detail of a compact imbalanced MZI based on TIR mirrors; (c) SEM picture of Euler bends with L and U shape and detail of a spiral waveguide using larger L-bends.

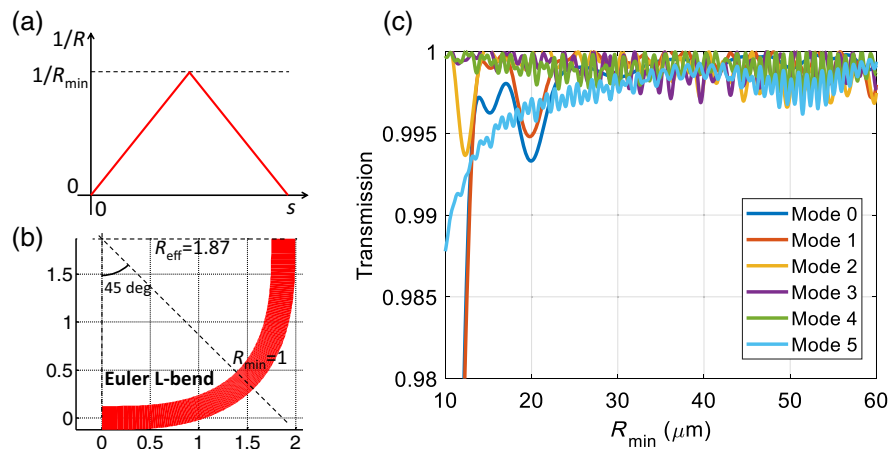


Fig. 6 (a) The linear change of the curvature $1/R$ as a function of the length s in an Euler bend, starting from zero, reaching up to $1/R_{\min}$ and then going back to zero symmetrically. (b) Example layout of a 90-deg Euler bend (or L-bend) with unity minimum bending radius, showing the resulting effective radius R_{eff} . (c) Simulation of the transmission of the TE_{00} mode and of five horizontal higher-order TE modes of a 1.5- μm -wide strip waveguide at the output of a 90-deg Euler bend as a function of the minimum bending radius. The five HOM TE_{n0} modes ($n = 1, \dots, 5$) have n nodes in the horizontal direction and zero nodes in the vertical direction. The wavelength is 1.55 μm .

strain can be easily compensated by fine-tuning the waveguide width.

Most of the building blocks, including multimode interference (MMI) splitters, can be designed to support both polarizations at the same time. On the other hand, in many applications (including telecom and sensing), polarization can be used as a degree of freedom, in which case a polarization splitter/combiner is needed and preferably also different types of polarization rotators. We are presently developing a wide portfolio of building blocks for polarization management, including MZI polarization beam splitters (PBSs)^{13,38} [see Fig. 7(a)] and rotators.³⁹ Remarkably, we have demonstrated the use of silicon itself as a magneto-optic material and achieved Faraday rotation in zero-birefringence waveguides.¹⁴ Our ultimate goal is to build

a fully integrated all-silicon circulator based on splitters/combiners and reciprocal and nonreciprocal rotators [Fig. 7(b)].

We conclude this section by mentioning that Faraday mirrors are commonly used in quantum photonics, including QKD systems (see Sec. 3), to ensure stable operation,^{40,41} as the polarization of the reflected light is always orthogonal to the input polarization (i.e., antipodal on the Poincaré sphere).⁴² Faraday mirrors can be achieved in the platform by combining an FR with a back-reflector, such as an MMI reflector or a Sagnac loop.⁴³

2.1.5 Low-loss wavelength filters

We have demonstrated several different types of wavelength filters, including ring resonators with Q up to 14 million,^{9,12}

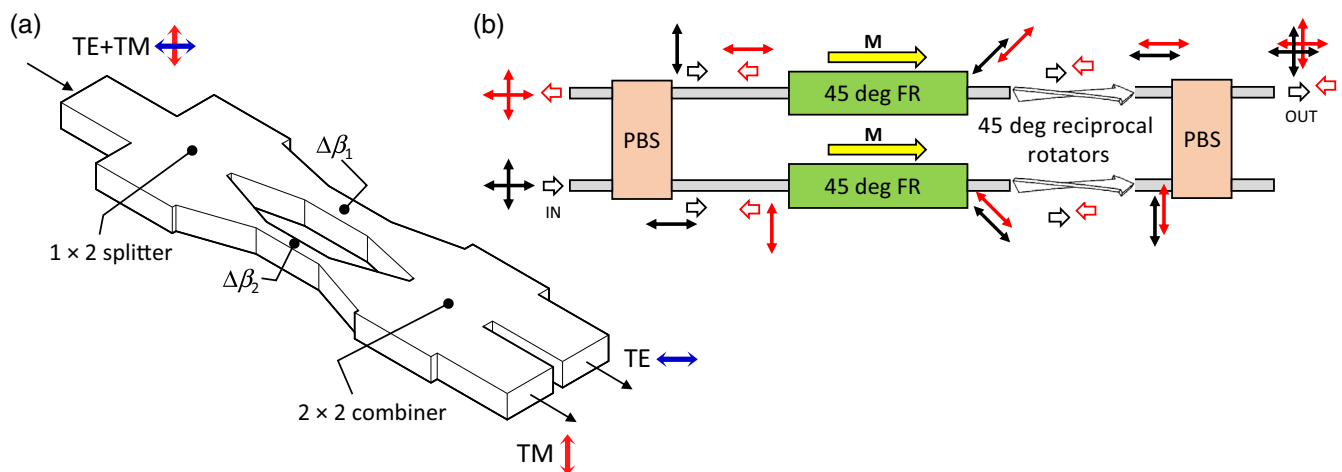


Fig. 7 (a) Sketch of an MZI exploiting the form birefringence of waveguides of different widths to serve as a PBS. (b) Scheme of a possible implementation of an integrated light circulator by combining PBSs, FRs, and reciprocal polarization rotators on chip.

compact MMI resonators,⁴³ flat-top lattice filters,⁴⁴ and flat-top ring-loaded MZIs.⁴⁵ Some of these filters can be designed to have <0.5 dB excess loss. We have also demonstrated low-loss echelle gratings and arrayed waveguide gratings (AWGs)⁴⁶. In Fig. 8(a), we show the layout of an A WG with a small footprint due to the use of Euler bends. The device is polarization-independent because of the incorporation of strip waveguides with a square cross section. Excess loss is in the 2- to 3-dB range, and the extinction ratio (ER) is larger than 25 dB. We have also demonstrated AWGs with loss in the 1- to 2-dB range,⁴⁶ and an ER exceeding 30 dB on all channels. We are presently working on further reduction of excess loss by improving design and fabrication of the star coupler. For echelle gratings like the one shown in Fig. 8(a), we have already demonstrated excess loss lower than 1 dB for both polarizations with an ER exceeding 20 dB for all channels.

2.1.6 Interfacing micro- and nanoscale devices

The low propagation loss of micron-scale waveguide technology comes with the price of weak interaction with any element integrated directly on top of the waveguides. This problem has been successfully addressed with different fabrication techniques that do not jeopardize the performance of the platform. For example, recently we have been developing a light escalator⁴⁷ made of hydrogenated amorphous silicon (a-Si:H) to interface micron-scale waveguides with submicron waveguides, thin layers including 2D materials, and superconducting nanowires. We grow a submicron layer of a-Si:H (refractive index around 3.65) on top of the crystalline device layer (refractive index around 3.48 at a 1550 nm wavelength), and pattern it to achieve adiabatic light coupling. The simulation in Fig. 9(a) shows how the light propagates from the thick silicon waveguide to the thinner a-Si:H layer. The a-Si:H layer thickness can be optimized to maximize the overlap of the propagating light with, e.g., a graphene layer (for applications such as light detection⁴⁸ or modulation⁴⁹) or a superconducting nanowire single-photon detector⁵⁰ (SNSPD, also see Sec. 2.2) sandwiched between crystalline silicon (c-Si) and a-Si:H, similar to what is sketched in Fig. 9(b). Furthermore, crystalline silicon can also be selectively removed and replaced with a deposited silica layer before depositing the a-Si:H layer, as sketched in Fig. 9(c). The resulting high-index contrast a-Si:H waveguide allows us to interface the micron-scale waveguide with submicron waveguides including plasmonic slot waveguides or even just PICs based on submicron silicon waveguides that can be simply bonded on top of the a-Si:H waveguide and evanescently coupled via inverse

tapers. Both types of escalators can be fabricated using the same fabrication process. Another unique opportunity to couple microscale waveguides to nanophotonic devices comes from the URM. In fact, there are cases requiring the light to propagate across a functional surface (unlike the escalator case, where it propagates along it). In these cases, functional surfaces can be fabricated or just transferred on top of the flat output surface of the mirror (which is made of crystalline smooth silicon, not etched). This is a straightforward way to integrate metasurfaces, including waveplates,⁵¹ metalenses,⁵² or electro-optic modulators.^{53,54} However, the limited size of the mirror (3 μm in the waveguide propagation direction, i.e., a few wavelengths) may present a challenge for the design of the metasurface.

2.2 Active Building Blocks

We can divide the active elements in two main categories: electrical-to-optical converters (EOCs), which, in the thick-SOI platform, are basically all phase shifters (either thermo-optic or electro-optic) and OECs, i.e., photodetectors.

2.2.1 Phase shifters

We implement thermo-optic phase shifters by implanting a thin silicon pedestal at the bottom of strip waveguides [Fig. 10(a)]. We usually cut away the remaining part of the pedestal to achieve lower power consumption, reaching about 25 mW per π -shift, with both rise time and decay time of about 15 μs (i.e., a speed of about 66 kHz). Very recently, we have also demonstrated ~ 2 mW per π -shift (not yet published) by fabricating the heaters on special cavity-SOI wafers, which limits the heat flow through the substrate.

Placing the heaters in direct contact with the silicon layer ensures a significant reduction of thermal cross talk⁵⁵ compared to heaters based on metal wires placed on top of the waveguide upper cladding. This is a major advantage for complex circuits requiring several thermo-optic phase shifters. By design, thermo-optic phase shifters come with no excess loss.

When higher speed is needed, we can reach about 2–3 MHz using simple PIN junctions, with only one implantation level, as sketched in Fig. 10(b). In this case, the refractive index changes due to carrier injection inducing plasma dispersion.⁵⁶ The power consumption for a π -shift is lower than 5 mW. Nevertheless, plasma dispersion inherently adds amplitude modulation on top of the phase modulation, due to the Kramers–Kronig relations.²⁹ The loss associated with a π -shift is on the order from 1 to 2 dB.

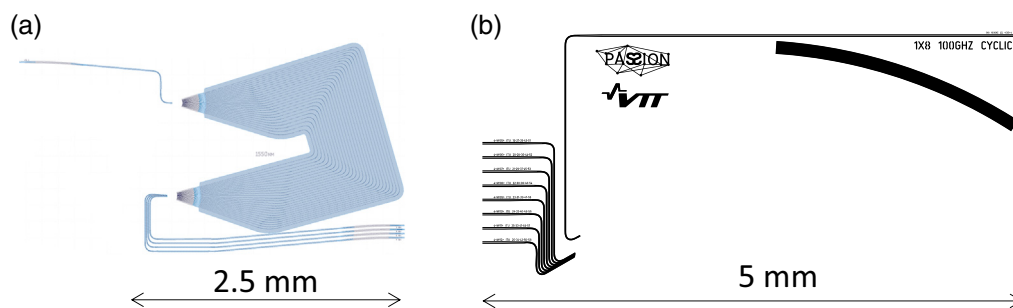


Fig. 8 (a) Compact AWG with 100-GHz channel spacing and 5-nm free spectral range exploiting Euler bends and nearly zero birefringence waveguides, ensuring polarization-independent operation. (b) Cyclic echelle grating with 100-GHz channel spacing.

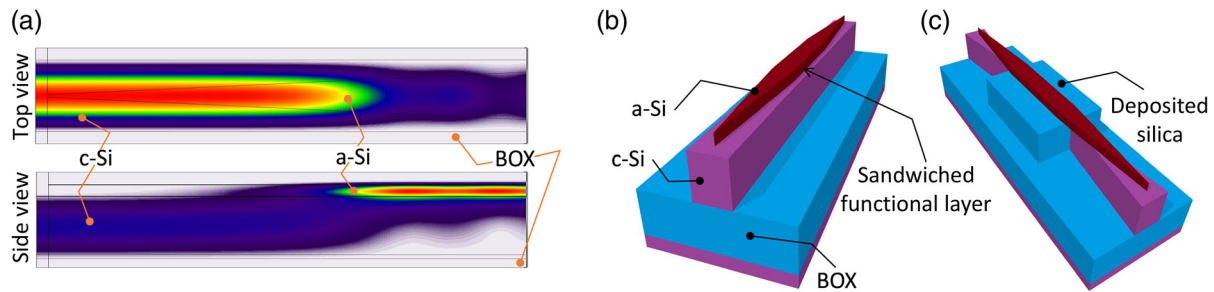


Fig. 9 (a) 3D simulation using the eigenmode expansion method of the adiabatic power transfer from a $3\text{-}\mu\text{m}$ thick c-Si waveguide to a 400-nm thick and $200\text{-}\mu\text{m}$ long a-Si:H tapered waveguide fabricated on top. (b) 3D sketch of two escalators to couple light to the a-Si:H waveguide and then back to the $3\text{-}\mu\text{m}$ thick waveguide, showing where a functional layer can be sandwiched between the two silicon types in the region where the light is guided in a-Si:H. (c) A different type of escalator to couple light to submicron waveguides.

Indeed, when made sufficiently long, the same type of PIN junction is also used for variable optical attenuators.⁵⁷

To overcome these limitations, we are also developing phase modulators relying on the so-called electric-field-induced Pockels effect [EPIPE, see Fig. 10(c)],⁵⁸ in close collaboration with the University of Tokyo. For these modulators, we expect significantly lower excess loss due to the high-reverse bias (electric field of about $40\text{ V}/\mu\text{m}$, as close as possible to the breakdown). In particular, we do not expect any major amplitude modulation associated with phase modulation. Furthermore, we aim to reach modulation speeds exceeding 1 GHz and possibly approaching 10 GHz . We also expect the power consumption to be in the microwatt range per π -shift, which is important for cryogenic applications. In fact, EPIPE works well also at cryogenic temperatures⁵⁹ because it is not affected by carrier freeze-out, unlike plasma dispersion.⁶⁰

With the goal of achieving extremely low-power consumption in combination with modulation speeds exceeding 100 GHz , we are also developing plasmonic modulators in collaboration with ETH Zürich and the company Polariton Technologies.⁶¹ In addition to the conventional approach based on nonlinear polymers, we are also exploring the possible use of a-Si:H as nonlinear material based on EPIPE.⁶² We point out that plasmonic

modulators are also particularly suitable for cryogenic applications,⁶³ since they do not rely on charge carriers and operate with ultralow power dissipation.⁶⁴ The main limitation of plasmonic phase shifters is the high excess loss, typically exceeding 5 dB . However, as explained in Sec. 3, this can be acceptable in some applications.

To conclude this section, we point out that a key missing building block for quantum PICs (QPICs) in all platforms is a suitable phase shifter to simultaneously enable a small footprint, ultralow power consumption, high-speed, ultralow optical loss, and cryogenic operation, or at least a subset of these properties, depending on the application. Recent results demonstrate that using microelectromechanical systems is a promising path for both submicron silicon⁶⁵ and silicon nitride^{66,67} platforms. This approach can result in losses below 0.5 dB , speeds from a few MHz to beyond 100 MHz , and footprints ranging from about $100\text{ }\mu\text{m} \times 100\text{ }\mu\text{m}$ to $1\text{ mm} \times 1\text{ mm}$. One additional avenue, which we are presently exploring for faster and more compact phase shifters, is to place electro-optic metasurfaces^{53,54} on top of URMs. Here the goal is to access the full nonlinear coefficient of electro-optic polymers, which is typically reduced by one order of magnitude in plasmonic slot waveguides.⁶⁸

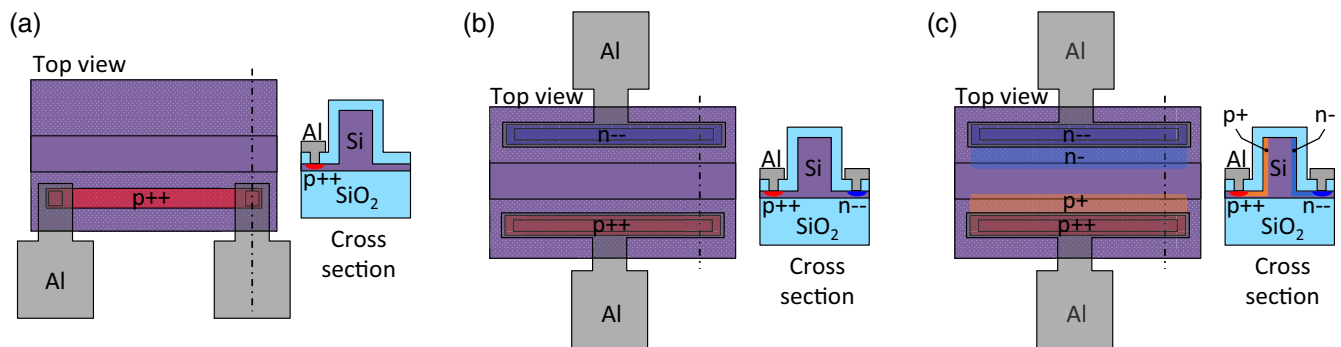


Fig. 10 Top views and cross sections of the three main types of phase shifters available on the platform: (a) thermo-optic (also see Fig. 1); (b) electro-optic, based on plasma dispersion through carrier injection in a PIN junction; (c) electro-optic, based on EPIPE with a high-inverse bias voltage through a PIN junction.

2.2.2 Detectors

The platform includes monolithically integrated germanium (Ge) photodiodes (PD), with responsivity on the order of 1 A/W at a 1550 nm wavelength, meaning 80% quantum efficiency. We have developed both high-speed PDs and monitor PDs. The high-speed PDs exceed 40-GHz speed when operated with 1-V reverse bias,¹⁰ with a dark current of about 4 μ A, whereas monitor PDs are operated with lower bias voltage and have about 10-nA dark current with about 1-GHz speed. We are presently starting cryogenic characterization of the PDs to determine the temperature dependence of dark current,⁶⁹ responsivity, signal-to-noise ratio,⁷⁰ speed, carrier freeze-out, and wavelength range of detection. We are also developing avalanche photodiodes⁷¹ exploiting the avalanche effect in silicon⁷² and also plan to operate them in Geiger mode to achieve single-photon avalanche detectors.⁷³

Additionally, in collaboration with ETH Zürich, we are also developing high-speed plasmonic Ge detectors to exceed 500 GHz analog bandwidth.^{74,75} Here the main driver is not the detection efficiency but high-speed operation at a few deg. Kelvin, with the goal of developing suitable OECs to transfer a large amount of data to the cryostat. As explained in more detail in Sec. 4, the idea is to drive superconducting electronics (e.g., single-flux quantum, SFQ) using optical fibers.

With cryogenic and quantum applications in mind, we are also developing guided-wave SNSPDs, with the final goal of coupling them through a light escalator [Fig. 9(b)]. In order to speed up the detector development, we have started fabricating the devices sketched in Fig. 11(c). We first oxidized a silicon wafer, deposited superconducting NbN on the thermal oxide, and patterned the nanowires using e-beam lithography, as shown in Fig. 11(a). Next, we deposited a-Si:H and patterned the waveguides [Fig. 11(b)] including inverse tapers to improve fiber coupling from the chip edge. The optical fiber is aligned using a nanopositioner in the cryostat. In parallel, we are also developing amorphous alternatives^{76,77} to crystalline NbN, targeting improved fabrication yield of the detectors.

The SNSPD is the closest thing to an ideal single-photon detector demonstrated to date, with detection efficiencies exceeding 97% extending into the telecom wavelength range,⁷⁸ speeds in the GHz range,⁷⁹ jitter even lower than 3 ps,⁸⁰ and dark counts under 0.1 Hz.⁸¹ However, for some quantum realizations,^{82–84} and especially those based on Gaussian states, photon number resolution (PNR) is an important capability that is not easily addressed by SNSPDs. A possible solution is transition edge sensors (TESs),⁸⁵ but their speed is presently limited to about

1 MHz. Unfortunately, TESs require temperatures on the order of 100 mK, which cannot be achieved with closed-cycle tabletop cryostats but require more complex and bulky sub-Kelvin coolers, such as dilution refrigerators.

However, it should be noted here that solid-state cooling technology developed currently at VTT can provide a viable solution to integrate also compact sub-Kelvin refrigerators in the future.^{86,87} These coolers are superconductor—silicon hybrid chips that can be directly connected to the PIC with 3D-integration schemes, such as flip-chip bonding. This would enable sub-Kelvin operation temperature for the circuits inside simple, cost-effective, and compact pulse-tube systems.

Integration of TESs on optical waveguides has already been demonstrated on other platforms.^{88,89} Our integration approach is in line with what we explained above for SNSPDs and leverages the TES pixel⁹⁰ and SQUID-based readout technology⁹¹ developed at VTT. From a broader perspective, the in-house integrated superconducting device technology based on Nb cross junctions⁹² can provide interesting opportunities for the quantum upgrade of the micron-scale platform (also see Sec. 4). For example, we presently use the technology for the TES readout circuits,⁸⁹ SQUID magnetometers,⁹³ and different Josephson parametric devices.^{94–96} Furthermore, in collaboration with the Royal Institute of Technology KTH and with the company Single Quantum, we are also exploring the possible use of single SNSPDs as efficient PNR detectors.^{97–99}

2.3 Hybrid Integration

Several different PIC technologies are available, including most mature submicron and micron-scale silicon and silicon nitride²⁰ platforms, and micron-scale indium phosphide¹⁰⁰ platforms, as well as the more recent lithium niobate on-insulator platforms^{101–104} and compound-on-insulator platforms.¹⁰⁵ Each material system comes with its strengths and weaknesses, and suitable combinations of complementary systems are thus often needed to achieve fully integrated solutions. A quintessential case is the lack of monolithically integrated light sources in all platforms not based on compound semiconductors, where either heterogeneous integration¹⁰⁶ or hybrid integration^{7,107} is needed to generate light on chip.

Our main focus at VTT is on hybrid integration based on high-precision flip-chip bonding at the wafer scale, which is suitable for mid-volume production in a complementary metal oxide semiconductor (CMOS) fabrication facility like ours. Unlike with heterogeneous and monolithic integration, in the

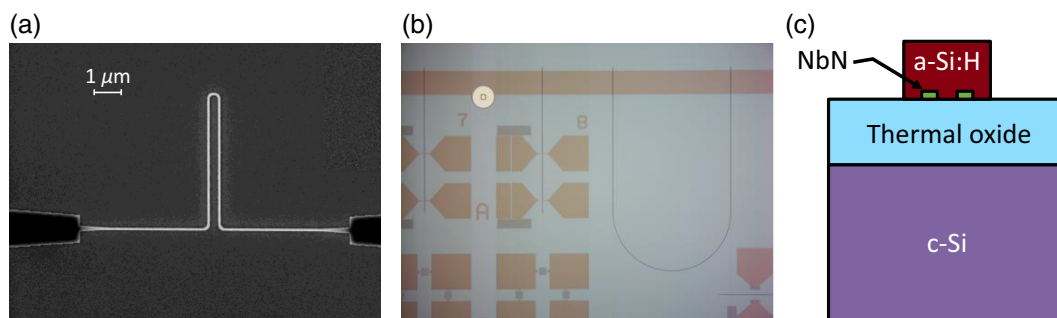


Fig. 11 (a) SEM picture of a fabricated NbN SNSPD before a-Si:H deposition; (b) micrograph of a detail of a fabricated chip after etching the a-Si:H waveguides; (c) sketched cross section of an a-Si:H waveguide with the NbN nanowire embedded (in green).

hybrid approach, the silicon process and the III-V process (or the process of any other complementary material system) can happen in parallel in two different fabrication facilities, which comes with several advantages. These include shorter overall lead time, reduced process flow complexity, reduced constraints and trade-offs for the two material systems, and decoupled yield of the two processes, resulting in higher overall yield, i.e., higher cost efficiency. Another advantage of hybrid integration is that it is not bound to the constraints that may arise in monolithic integration regarding, e.g., CMOS compatibility and thermal budgets. Furthermore, hybrid integration can be made with commercially available dies (e.g., light sources or photodetectors) which can lead to even higher cost efficiency.

Using either vertical facets or URMs, we can easily integrate devices where light propagates, respectively, in-plane, such as distributed Bragg reflector lasers, semiconductor optical amplifiers, or electro-absorption modulators, or out-of-plane, such as vertical cavity emitting lasers or free-space photodetectors. In particular, the URM can be a key component for QPICs, as it is extremely low-loss, broadband, and polarization-independent. For example, it can be used to efficiently couple light from deterministic single-photon sources based on quantum dots in vertical cavities¹⁰⁸ or to couple single photons or Gaussian states to arrays of short SNSPDs [see Fig. 12(b)]. We stress here that, even though we have a clear path to monolithic integration of SNSPDs (see Sec. 2.2), based on the above considerations, hybrid integration will be the most efficient integration approach for large SNSPD arrays until we develop a SNSPD fabrication process with sufficiently high yield.

3 QKD Receivers

A first example application that can be enabled by the thick-SOI platform is QKD networks¹⁰⁹ with higher key rates and/or longer working distance. In fact, PIC solutions are in the product roadmap of major QKD players,¹¹⁰ because of their unmatched stability and scalability. Indeed, several examples of PIC-based implementations have been reported to date, covering different types of QKD schemes.^{111–119} We have identified a clear path for how the platform could support the development and large-scale deployment of high-performance QKD systems for both

discrete variable (DV) QKD and continuous variable (CV) QKD, as briefly presented in the following.

3.1 DV-QKD

DV-QKD systems are most suitable to cover long distances. The longest QKD link reported to date reached 830 km using a special configuration with a central node,^{120,121} whereas the longest point-to-point link exceeded 400 km¹²² (corresponding to about 70 dB loss in ultralow loss fibers). The best commercial systems are typically limited to the 100- to 150-km range, mainly to ensure secure communication with key rates high enough to be useful. In fact, in the DV-QKD implementations most suitable for long distances, the key rate scales linearly with the link transmission probability η , which is the probability of a transmitted photon being detected at the receiver, accounting for all possible transmission and coupling losses as well as the limited detector efficiency.¹²³ In stark contrast to classical optical communication links, such key rate scaling implies a large mismatch between the transmission speed and the detection speed. In other words, the detector can be orders of magnitude slower than the modulator, which is a unique opportunity to combine the fastest ever achieved optical modulators with the most efficient single-photon detectors demonstrated to date, namely plasmonic modulators and SNSPDs, respectively. Transmitter speeds of present QKD systems are on the order of a few GHz, meaning that plasmonic phase and amplitude modulators could be used to boost the key rate by at least two orders of magnitude, while being still well-matched by SNSPDs on the receiver side. In fact, present commercial SNSPDs can easily exceed 10-MHz count rates with more than 80% detection efficiency and will possibly exceed GHz count rates and 95% detection efficiency in the future. We stress that the high losses of plasmonic modulators, which are a strong limitation for classical optical communication, are not at all a problem for practical DV-QKD transmitters, which are based on strongly attenuated light sources. On the other hand, high losses are not tolerable for the receiver, so plasmonic modulators are not an option for protocols (such as the standard BB84) where modulators are also needed to choose the measurement basis on the receiver side. Nevertheless, this is not a strong limitation, given that the most robust protocols for

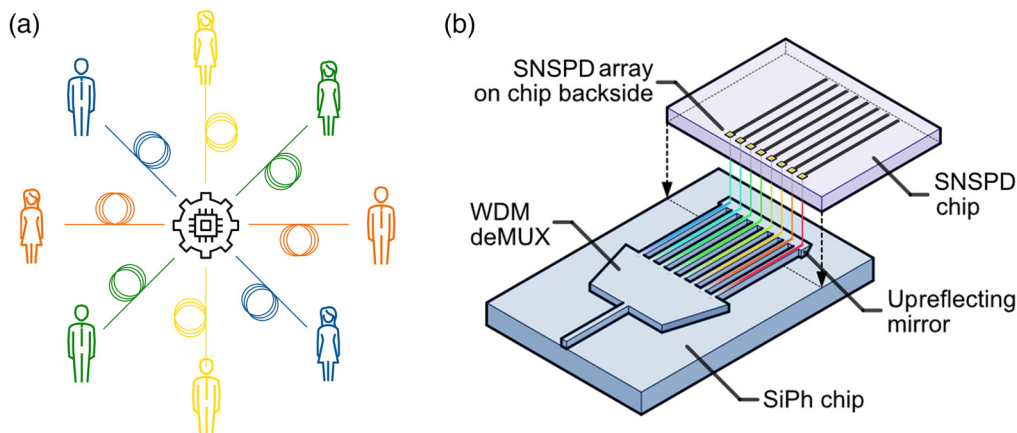


Fig. 12 (a) Schematic representation of QKD implementations based on a central node for photon detection where all the users are equipped with suitable and low-cost transmitters. (b) 3D sketch of the solution we are developing with our partner Single Quantum to address arrays of SNSPDs with low-loss and high-fabrication yield.

practical DV-QKD rely on passive receivers, requiring no modulators.^{122,124,125}

The combination of plasmonic modulators and SNSPDs becomes even more attractive when considering that some of the most promising DV-QKD protocols, including measurement-device-independent (MDI) QKD^{126,127} and twin-field QKD^{120,123}, connect the users through a central unit (completely untrusted) where all the photon detections occur [Fig. 12(a)]. Large-scale deployment of these systems can be achieved by providing all users with low-cost transmitters (achievable with plasmonic chips) while deploying a central detection unit, owned by the operator, to host a table-top closed-cycle cryostat where thousands of SNSPDs can be economically cooled down and operated in parallel. In this vision, the cryostat would be connected to tens to hundreds of fibers, and each fiber should carry tens to hundreds of wavelength division multiplexed (WDM) signals.

To this end, at VTT we are presently fabricating low-loss AWGs to demultiplex the WDM signals coming from a single fiber and couple them to flip-chip-bonded arrays of SNSPDs designed and fabricated by Single Quantum to match our layout [see Fig. 12(b)]. Monolithic integration of AWGs and SNSPDs has been already demonstrated¹²⁸ but with high losses both for fiber coupling and demultiplexing. Furthermore, monolithic integration of large SNSPD arrays is still challenging, due to the relatively poor SNSPD fabrication yield. Hybrid integration of SNSPD chips (with only two detectors) has been recently demonstrated with submicron silicon waveguides¹²⁹ for time multiplexed MDI-QKD. The coupling losses demonstrated therein were very high, as grating couplers were used to couple both the optical fiber and the SNSPDs. We instead aim at a solution simultaneously ensuring high yield, broadband low-loss fiber coupling, and low demultiplexing loss, which can be even made polarization-insensitive with a suitable design of the SNSPD geometry.^{130,131} The final goal is full monolithic integration of a DV-QKD receiver on the thick-SOI platform, providing much better and more stable control of relative phase and time jitter, therefore leading to higher fringe visibility.

3.2 CV-QKD

An alternative approach is CV-QKD, which relies on Gaussian states instead of single photons. The main advantage is that its implementation⁴¹ requires only standard telecom components used for classical coherent optical communication, and, in particular, there is no need for single-photon detectors. The main drawback is that secure implementations scale quadratically with the transmission probability η , which limits the operation range to about 50 km (or to be more rigorous, 10-dB loss, assuming standard 0.2 dB/km fiber loss). Furthermore, unlike DV-QKD, the receiver speed must match the transmitter speed. On the transmitter side, plasmonic modulators are again the perfect choice, given that their losses can be easily tolerated, and they can easily achieve both phase and amplitude ultrafast modulation simultaneously.⁶⁴ Ultrafast phase modulation is needed also on the receiver side, but only on the local oscillator and not on the quantum states,⁴¹ meaning that some modulator losses are acceptable. Detection is typically done using shot-noise-limited balanced pulsed homodyne detectors⁴¹ whose operation speed and stability can greatly benefit from PIC integration and dedicated electronics.¹³²

We, therefore, plan to exploit fast Ge PDs in combination with our in-house expertise in ultrafast electronics^{133,134} to develop balanced photodetectors with a speed above 50 GHz. We stress that even though the speed of our present Ge PDs is limited to about 40 GHz, suitably designed Ge PDs with smaller volumes have been recently demonstrated to reach up to 265 GHz.¹³⁵ In our vision, the CV-QKD receiver will be monolithically integrated on our thick-SOI platform, to include the ultrafast plasmonic phase modulator and the balanced photodiode. Also in this case, the PIC will ensure much better and more stable control of relative phase and time jitter compared to realizations based on optical fibers, therefore, leading to improved overall performance of the whole QKD system.

On the transmitter side, integration of the plasmonic devices on our platform would not be strictly necessary, but it could improve operation stability, e.g., through integrated Faraday mirrors (see Sec. 2.1) not available in any other PIC platform. Similar considerations apply to DV-QKD transmitters. Indeed, many practical implementations of both DV- and CV-QKD rely on Faraday mirrors.^{41,122,125}

The platform can also support quantum communication applications beyond QKD. A promising path is the development of acousto-optical devices to efficiently transduce superconducting qubits or spin qubits into optical qubits and vice versa. Such transducers would allow us to connect quantum processors via optical quantum states in optical fibers and create more powerful quantum computers based on multi-quantum-processor architectures, even using quantum computers located several kilometers away. With this application in mind, together with the University of Bristol, we are exploring the possible realization of efficient piezoelectric microwave-to-optical transducers.¹³⁶

4 Scaling-Up Cryogenic Quantum Computers

A second example application is the use of optical fibers to transfer data to and from superconducting quantum computers, aiming to scale up the number of qubits and achieve useful universal quantum computing. We are currently in the “noisy intermediate-scale quantum” era,¹³⁷ which means that significant applications are expected already in the short- and medium-term with a limited number of noisy qubits. However, it is generally agreed that universally useful quantum computers will require about one million qubits.¹³⁸

To date, the most advanced universal quantum computers are based on superconducting qubits and operated at temperatures below 50 mK, which is required to minimize thermal noise. A highly scalable approach based on silicon qubits is also quickly evolving^{139–143} and requires low temperatures as well. In all cryogenic quantum processors, electrical transmission lines are used to carry the electrical signals driving and reading the qubits inside the cryostat. Even though this approach is feasible when dealing with a few hundreds of qubits, it becomes challenging for thousands of qubits and not viable anymore when approaching one million qubits. In fact, electrical cables come with a detrimental trade-off between bandwidth and thermal conductivity. For these reasons, at VTT, we are intensely developing the next generation of communication interfaces for cryogenic qubits, using optical fibers and suitable OECs and EOCs.

There are at least two significantly different research directions for the optical control of superconducting quantum technology: (i) a number of OECs generate the drive signals of

a quantum computer at the cryogenic temperature. Here the OEC must receive an optical signal from room temperature that is directly suitable for driving the qubits and their gates. (ii) A number of cryogenic OECs receive digital optical input signals and convert them into digital electrical signals driven into a superconducting SFQ device.¹⁴⁴ The SFQ is a superconducting processor for classical data that can also generate drive signals for the quantum computer, as shown in Fig. 13. The packaging density (crucial for scaling up) of both approaches can be supported by integrated optical techniques, such as WDM for multiplexing multiple signals into the same optical fiber.

The control of qubits has already been demonstrated for the first approach.¹⁴⁵ This approach benefits from the possibility of using existing electrical qubit drive electronics whose signals are simply converted into an optical form with an EOC at room temperature. However, at the small signal levels required by quantum computers, OECs suffer from shot noise, which can be detrimental for driving their analogue signals into sensitive quantum computers. The second approach is significantly more tolerant to shot noise, since the OECs only need to generate digital signals for SFQ, which can generate quantized analogue signals based on digital input data.

Our vision follows this second approach, illustrated in Fig. 13, where a large amount of data from a supercomputer is serialized by a suitable EOC and sent through an optical fiber to a cryogenic OEC to drive SFQ logic.¹⁴⁴ After inputting the data into the quantum processor, the SFQ co-processors use the calculation output to drive a suitable cryogenic EOC that, through another optical fiber, sends the results to a deserializing OEC that communicates back to the supercomputer.

The serializer and deserializer are in general needed because the speed of SFQ logic is typically much higher than the speed of standard CMOS electronics. SFQ is a promising choice due to its ultralow energy dissipation, which is mandatory when working at the ultralow temperatures required by superconducting quantum computers.

CMOS electronics can also be used in cryogenic environments, where low temperatures allow lower operating voltages and thus lower power consumption.^{146,147} Cryo-CMOS uses traditional CMOS components that are tailored toward low-temperature operation. However, with CMOS circuits, it is very

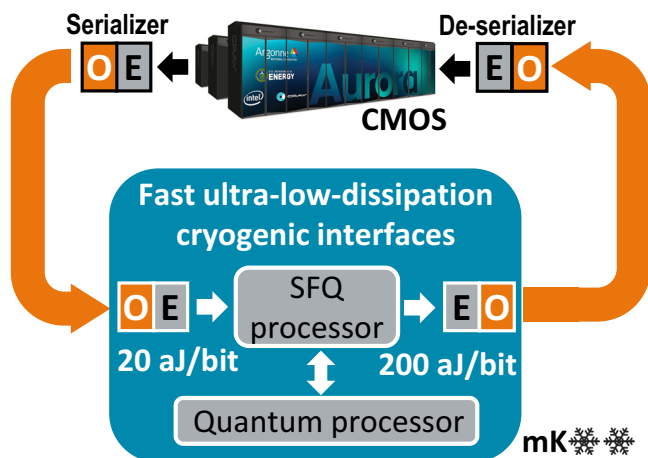


Fig. 13 Schematic representation of our plans to use optical fiber links to interface cryogenic quantum computers with supercomputers.

hard to have sufficiently small dissipation. For example, the total power dissipation of only two-spin qubit processor read-out and control circuitry operated at 3 K was 330 mW,¹⁴⁸ which is already on the high end of the tolerance level of the modern cryostats. Furthermore, reaching high enough clock rates (>1 GHz) at low temperature is a significant challenge that, if not solved, implies higher qubit overhead. The strong points of the cryo-CMOS technology are the existing fabrication infrastructure and the advanced design tools and expertise.

More dramatic gains in energy efficiency are possible using SFQ technology. This technology and its variants, such as energy efficient SFQ, represent bits as short (≈ 1 ps) pulses produced by switching processes in superconducting tunnel junctions called Josephson junctions. The typical energy of these pulses is only 0.2 aJ, and the pulses can be processed at speeds exceeding 100 GHz.¹⁴⁹ In the past, their use has been limited by the requirement of cryogenic temperature operation and mediocre packing density of components. For qubit interfacing purposes, neither of these issues is relevant. Superconducting electronics based on SFQ logic dissipates $<1\%$ of the energy dissipated by CMOS electronics¹⁵⁰ and enhanced variants (eSFQ or eRSFQ logic) can even dissipate $<0.1\%$ compared to the CMOS systems. SFQ controllers additionally enable vastly superior clock frequencies, in extreme cases even above 700 GHz.¹⁵¹ With advanced thermal management, the SFQ controllers could be even directly integrated with the qubit processor altogether removing the need for very complex cabling solutions.

As part of this vision, we are presently developing, together with our partners, several PIC solutions for different building blocks. For example, in Fig. 14, we show a long-term vision of how to replace a prototype serializer, presently based on optical fibers and discrete components, with a fully integrated PIC solution. A III-V reflective semiconductor optical amplifier, including a saturable absorber, is flip-chip bonded on the silicon chip where it is coupled to an integrated, compact, and low-loss external cavity to create an integrated mode-locked laser (IMLL). The generated wavelengths are then separated by a low-loss integrated demultiplexer. The signal in each waveguide is finally modulated independently through an array of amplitude modulators, each driven by relatively slow electrical signals (from 1 to 2.5 GHz). The resulting signals are first delayed by multiples of a suitable delay unit and finally recombined through a wavelength multiplexer. We are presently developing passive PICs combining the delay lines and the final multiplexer. We will test them as part of the free-space serializer prototype we have already built.

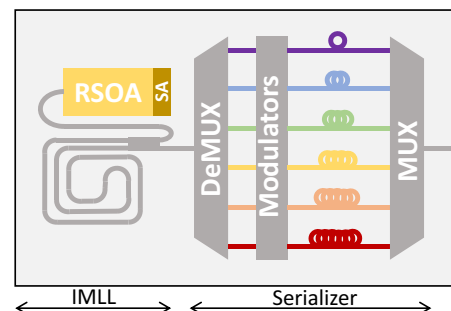


Fig. 14 Long-term vision of a PIC based serializer, including an IMLL as a multiwavelength light source.

A second example is the cryogenic OEC that we are building using SNSPDs. In this particular application, we are more interested in their detection speed rather than extremely high detection efficiency, given that we can afford to use multiple photons per pulse. Together with our collaborators, we are trying to achieve the ultimate SNSPD speed. A simple approach is to make the nanowire as short as possible, but experimental results clearly show that latching^{152–154} becomes an issue in doing so. Active electrical quenching has also been proposed but without dramatic improvements.¹⁵⁵ In order for the OEC speed to approach the SFQ speed, we are also exploring different multiplexing approaches, addressing arrays of SNSPDs instead of single detectors. In this approach, we avoid using the optical serializer at room temperature and replace it with an electrical serializer inside the cryostat,¹⁵⁶ resulting in major underexploitation of the fiber bandwidth. The simplest brute force approach is space division multiplexing, i.e., coupling each SNSPD with a dedicated fiber. We are indeed developing 2D fiber arrays suitable for cryogenic illumination of detector arrays. A finer approach is to use WDM the same way as in Fig. 12(b), where a single fiber carries several wavelengths. Time division multiplexing could also be an option, but it would require active control of a network of relatively fast switches.

The most demanding part of the vision in Fig. 13 is by far the cryogenic EOC. In fact, the energy and the voltages available from the SFQ electronics are very low (attojoules per bit and microvolt, respectively), and thus driving a fast optical modulator inside the cryostat is very challenging. Even though plasmonic modulators have been demonstrated to work with <1 V and at attojoule the energy level,⁶⁴ driving them with SFQ is still nontrivial and requires some major development, which we are presently tackling.

Together with our partners, we are presently developing the SFQ processors in parallel as well as PIC-enabled EOCs and OECs, and we plan to start testing combinations of these different building blocks in the next few years as proofs of concept of our vision. In the long run, this will support the development of the Finnish quantum computer, which has recently achieved the first milestone of five qubits¹⁵⁷ and is now targeting 50 qubit superconducting quantum computer by 2024. At the same time, the same optical interfacing technology will help scale up also the customized silicon qubit platform that we are codeveloping.^{140,143}

5 Other Interesting Applications and Conclusions

To conclude, we briefly mention that the thick-SOI technology can support many other quantum technology developments. For example, we have just started a project with KTH to integrate their thin lithium niobate waveguides¹⁰⁴ on our platform. We have also ongoing discussions with Tampere University on how to exploit the multimode behavior and mode preservation capabilities of our PICs (see Sec. 2.1) to support spatial shaping of their qubits.^{34–36} We have also identified turbulence mitigation¹⁵⁸ for satellite QKD as a promising application of our low-loss PICs with efficient phase shifters and integrated responsive detectors. We additionally have an ongoing collaboration with the Max Planck Institute for Quantum Optics to implant erbium in our silicon waveguides to achieve quantum emitters with narrow linewidth.¹⁵⁹

We have introduced the thick-SOI platform with a special focus on the unique features that make it attractive for different quantum technologies, and we have also provided an overview of the ongoing developments to make it even more attractive in the near future. We presented two concrete cases elaborating in detail our vision of how PIC-based solutions will be able to support the large-scale deployment of high-performance QKD networks based on both DV-QKD and CV-QKD as well as the scaling-up of useful cryogenic quantum computers.

Acknowledgments

This work was supported by the European Union's Horizon 2020 Research and Innovation Program through projects aCryComm (Grant No. 899558), Quantum e-leaps (Grant No. 862660), OpenSuperQ (Grant No. 820363), EFINED (Grant No. 766853), and EMPIR SuperQuant (Project No. 20FUN07). We would like to acknowledge the support by the Academy of Finland Flagship Program, Photonics Research and Innovation (PREIN) (Decision No. 320168) and VTT Internal Quantum Initiative "Quantum leap in quantum control." This work was performed as part of the Academy of Finland Centre of Excellence program (Project No. 336817) and projects ETHEC (Grant No. 322580) and QuantLearn (Grant No. 350220). We also would like to acknowledge financial support from Business Finland through projects QuTI (No. 40562/31/2020) and PICAP (No. 44065/31/2020). We would like to thank our colleagues Emma Mykkänen, Tapani Vehmas, Giovanni Delrosso, Katja Kohopää, Markku Kapulainen, Pekka Pursula, Mikko Kiviranta, and Himadri Majumdar as well as our collaborators Val Zwiller, Mario Castañeda, Stephan Steinhauer, Samuel Gyger, Eva De Leo, and Stefan Köpfli for their inputs and fruitful discussions. The authors declare no conflicts of interest.

References

1. A. Acín et al., "The quantum technologies roadmap: a European Community view," *New J. Phys.* **20**(8), 080201 (2018).
2. J. Wang et al., "Integrated photonic quantum technologies," *Nat. Photonics* **14**(5), 273–284 (2020).
3. A. W. Elshaari et al., "Hybrid integrated quantum photonic circuits," *Nat. Photonics* **14**(5), 285–298 (2020).
4. S. Rodt and S. Reitzenstein, "Integrated nanophotonics for the development of fully functional quantum circuits based on on-demand single-photon emitters," *APL Photonics* **6**(1), 010901 (2021).
5. E. Pelucchi et al., "The potential and global outlook of integrated photonics for quantum technologies," *Nat. Rev. Phys.* **4**(3), 194–208 (2022).
6. G. Moody et al., "2022 Roadmap on integrated quantum photonics," *J. Phys. Photonics* **4**(1), 012501 (2022).
7. T. Aalto et al., "Open-access 3- μ m SOI waveguide platform for dense photonic integrated circuits," *IEEE J. Sel. Top. Quantum Electron.* **25**(5), 1–9 (2019).
8. A. Bera et al., "Ultra-low loss waveguide platform in silicon photonics," *Proc. SPIE* **12006**, 1200603 (2022).
9. Y. Marin et al., "Ultra-high-Q racetrack on thick SOI platform through hydrogen annealing," in *ECOC 2022 48th Eur. Conf. Opt. Commun.*, Basel, p. We4E.3 (2022).
10. T. Vehmas et al., "Monolithic integration of up to 40 GHz Ge photodetectors in 3 μ m SOI," *Proc. SPIE* **11285**, 112850V (2020).
11. M. Cherchi et al., "Dramatic size reduction of waveguide bends on a micron-scale silicon photonic platform," *Opt. Express* **21**(15), 17814–17823 (2013).

12. B. Zhang et al., "Compact multi-million Q resonators and 100 MHz passband filter bank in a thick-SOI photonics platform," *Opt. Lett.* **45**(11), 3005–3008 (2020).
13. D. Shahwar et al., "Polarization splitters for micron-scale silicon photonics," *Proc. SPIE* **11691**, 1169104 (2021).
14. D. J alas et al., "Faraday rotation in silicon waveguides," in *14th Int. Conf. Group IV Photonics*, IEEE, Berlin, pp. 141–142 (2017).
15. F. Gao et al., "A modified Bosch process for smooth sidewall etching," in *Proc. 22nd Micromech. Microsyst. Technol. Eur. Workshop*, Vestfold University College, Toensberg, pp. 69–72 (2011).
16. F. Gao et al., "Smooth silicon sidewall etching for waveguide structures using a modified Bosch process," *J. MicroNanolithogr. MEMS MOEMS* **13**(1), 013010 (2014).
17. R. A. Soref, J. Schmidtchen, and K. Petermann, "Large single-mode rib waveguides in GeSi-Si and Si-on-SiO₂," *IEEE J. Quantum Electron.* **27**(8), 1971–1974 (1991).
18. P.-I. Dietrich et al., "In situ 3D nanoprinting of free-form coupling elements for hybrid photonic integration," *Nat. Photonics* **12**(4), 241–247 (2018).
19. T. Aalto, "Broadband and polarization independent waveguide-fiber coupling," in *Silicon Photonics XVIII*, SPIE Press, pp. 12426–12440 (2023).
20. A. Rahim et al., "Open-access silicon photonics platforms in Europe," *IEEE J. Sel. Top. Quantum Electron.* **25**(5), 1–18 (2019).
21. G. Z. Mashanovich et al., "Low loss silicon waveguides for the mid-infrared," *Opt. Express* **19**(8), 7112–7119 (2011).
22. P. Karioja et al., "Integrated multi-wavelength mid-IR light source for gas sensing," *Proc. SPIE* **10657**, 106570A (2018).
23. C. Lindner et al., "High-sensitivity quantum sensing with pump-enhanced spontaneous parametric down-conversion," <https://arxiv.org/abs/2208.07595> (2022).
24. H. Rong et al., "Raman gain and nonlinear optical absorption measurements in a low-loss silicon waveguide," *Appl. Phys. Lett.* **85**(12), 2196–2198 (2004).
25. A. Gil-Molina et al., "Optical free-carrier generation in silicon nano-waveguides at 1550 nm," *Appl. Phys. Lett.* **112**(25), 251104 (2018).
26. B. Morrison et al., "Four-wave mixing and nonlinear losses in thick silicon waveguides," *Opt. Lett.* **41**(11), 2418–2421 (2016).
27. M. Pagani et al., "Low-error and broadband microwave frequency measurement in a silicon chip," *Optica* **2**(8), 751 (2015).
28. T. Aalto et al., "Total internal reflection mirrors with ultra-low losses in 3 μm thick SOI waveguides," *Proc SPIE* **9367**, 93670B (2015).
29. B. E. A. Saleh and M. C. Teich, *Fundamentals of Photonics*, Wiley, New York (1991).
30. M. Cherchi and T. Aalto, "Bent optical waveguide," WO2014060648 A1 (2014).
31. X. Jiang, H. Wu, and D. Dai, "Low-loss and low-crosstalk multimode waveguide bend on silicon," *Opt. Express* **26**(13), 17680–17689 (2018).
32. C. Li, D. Liu, and D. Dai, "Multimode silicon photonics," *Nanophotonics* **8**(2), 227–247 (2019).
33. A. Mohanty et al., "Quantum interference between transverse spatial waveguide modes," *Nat. Commun.* **8**(1), 14010 (2017).
34. F. Brandt et al., "High-dimensional quantum gates using full-field spatial modes of photons," *Optica* **7**(2), 98–107 (2020).
35. M. Piccardo et al., "Roadmap on multimode light shaping," *J. Opt.* **24**(1), 013001 (2021).
36. M. Hiekkamäki et al., "Observation of the quantum Gouy phase," *Nat. Photonics* **16**, 828–833 (2022).
37. Y. Wang, D. Dai, and D. Dai, "Multimode silicon photonic waveguide corner-bend," *Opt. Express* **28**(7), 9062–9071 (2020).
38. T. Aalto, "Devices and methods for polarization splitting," WO2020089530A1 (2020).
39. M. Harjanne, T. Aalto, and M. Cherchi, "Polarization rotator," WO2020225479A1 (2020).
40. H. Zbinden et al., "Interferometry with Faraday mirrors for quantum cryptography," *Electron. Lett.* **33**(7), 586–588 (1997).
41. P. Jouguet et al., "Experimental demonstration of long-distance continuous-variable quantum key distribution," *Nat. Photonics* **7**(5), 378–381 (2013).
42. M. Martinelli, "A universal compensator for polarization changes induced by birefringence on a retracing beam," *Opt. Commun.* **72**(6), 341–344 (1989).
43. M. Cherchi et al., "MMI resonators based on metal mirrors and MMI mirrors: an experimental comparison," *Opt. Express* **23**(5), 5982–5993 (2015).
44. M. Cherchi et al., "Flat-top interleavers based on single MMIs," *Proc. SPIE* **11285**, 112850G (2020).
45. M. Cherchi et al., "Fabrication tolerant flat-top interleavers," *Proc SPIE* **10108**, 101080V (2017).
46. S. Bhat et al., "Low loss devices fabricated on the open access 3 μm SOI waveguide platform at VTT," presented at *ECIO*, Ghent (2019).
47. A. Bera et al., "Amorphous silicon waveguide escalator: monolithic integration of active components on 3-μm SOI platform," *Proc. SPIE* **11285**, 1128507 (2020).
48. J. Goldstein et al., "Waveguide-integrated mid-infrared photodetection using graphene on a scalable chalcogenide glass platform," *Nat. Commun.* **13**(1), 3915 (2022).
49. M. A. Giambra et al., "High-speed double layer graphene electro-absorption modulator on SOI waveguide," *Opt. Express* **27**(15), 20145–20155 (2019).
50. W. H. P. Pernice et al., "High-speed and high-efficiency travelling wave single-photon detectors embedded in nanophotonic circuits," *Nat. Commun.* **3**, 1325 (2012).
51. Z. H. Jiang et al., "Broadband and wide field-of-view plasmonic metasurface-enabled waveplates," *Sci. Rep.* **4**(1), 7511 (2014).
52. M. Khorasaninejad and F. Capasso, "Metalenses: versatile multifunctional photonic components," *Science* **358**, eaam8100 (2017).
53. I.-C. Benea-Chelmus et al., "Electro-optic spatial light modulator from an engineered organic layer," *Nat. Commun.* **12**(1), 5928 (2021).
54. I.-C. Benea-Chelmus et al., "Gigahertz free-space electro-optic modulators based on Mie resonances," *Nat. Commun.* **13**(1), 3170 (2022).
55. S. Sabouri et al., "Thermo optical phase shifter with low thermal crosstalk for SOI strip waveguide," *IEEE Photonics J.* **13**(2), 1–12 (2021).
56. R. Soref and B. Bennett, "Electrooptical effects in silicon," *IEEE J. Quantum Electron.* **23**(1), 123–129 (1987).
57. D. W. Zheng, B. T. Smith, and M. Asghari, "Improved efficiency Si-photonics attenuator," *Opt. Express* **16**(21), 16754–16765 (2008).
58. E. Timurdogan et al., "Electric field-induced second-order nonlinear optical effects in silicon waveguides," *Nat. Photonics* **11**(3), 200–206 (2017).
59. U. Chakraborty et al., "Cryogenic operation of silicon photonic modulators based on the DC Kerr effect," *Optica* **7**(10), 1385 (2020).
60. M. Gehl et al., "Operation of high-speed silicon photonic micro-disk modulators at cryogenic temperatures," *Optica* **4**(3), 374 (2017).
61. M. Burla et al., "500 GHz plasmonic Mach-Zehnder modulator enabling sub-THz microwave photonics," *APL Photonics* **4**(5), 056106 (2019).
62. M. Cherchi, "Electro-optic plasmonic devices," WO2021099686A1 (2021).
63. P. Habegger et al., "Plasmonic 100-GHz electro-optic modulators for cryogenic applications," in *ECOC 2022 48th Eur. Conf. Opt. Commun.*, Basel, p. Tu1G.1 (2022).

64. W. Heni et al., "Plasmonic IQ modulators with attojoule per bit electrical energy consumption," *Nat. Commun.* **10**(1), 1–8 (2019).
65. P. Edinger et al., "Silicon photonic microelectromechanical phase shifters for scalable programmable photonics," *Opt. Lett.* **46**(22), 5671–5674 (2021).
66. T. Grottko et al., "Optoelectromechanical phase shifter with low insertion loss and a 13π tuning range," *Opt. Express* **29**(4), 5525–5537 (2021).
67. M. Dong et al., "High-speed programmable photonic circuits in a cryogenically compatible, visible-near-infrared 200 nm CMOS architecture," *Nat. Photonics*, **16**, 59–65 (2021).
68. H. Xu et al., "Design and synthesis of chromophores with enhanced electro-optic activities in both bulk and plasmonic-organic hybrid devices," *Mater. Horiz.* **9**, 261–270 (2021).
69. A. Pizzone et al., "Analysis of dark current in Ge-on-Si photodiodes at cryogenic temperatures," in *IEEE Photonics Conf., IPC*, pp. 1–2 (2020).
70. S. Siontas et al., "Low-temperature operation of high-efficiency germanium quantum dot photodetectors in the visible and near infrared," *Phys. Status Solidi A* **215**(3), 1700453 (2018).
71. Q. Zhang et al., "Low-loss and polarization-insensitive photonic integrated circuit based on micron-scale SOI platform for high density TDM PONs," in *Opt. Fiber Commun. Conf. Exhib., OFC*, pp. 1–3 (2017).
72. N. J. D. Martinez et al., "High performance waveguide-coupled Ge-on-Si linear mode avalanche photodiodes," *Opt. Express* **24**(17), 19072–19081 (2016).
73. P. Vines et al., "High performance planar germanium-on-silicon single-photon avalanche diode detectors," *Nat. Commun.* **10**(1), 1086 (2019).
74. Y. Salamin et al., "100 GHz plasmonic photodetector," *ACS Photonics* **5**(8), 3291–3297 (2018).
75. S. Koepfli et al., ">500 GHz bandwidth graphene photodetector enabling highest-capacity plasmonic-to-plasmonic links," in *ECOC 2022 48th Eur. Conf. Opt. Commun.*, Basel, p. Th3B.5 (2022).
76. E. Mykkänen et al., "Enhancement of superconductivity by amorphizing molybdenum silicide films using a focused ion beam," *Nanomaterials* **10**(5), 950 (2020).
77. M. Häußler et al., "Amorphous superconducting nanowire single-photon detectors integrated with nanophotonic waveguides," *APL Photonics* **5**(7), 076106 (2020).
78. J. Chang et al., "Detecting telecom single photons with 99.5–2.07+0.5% system detection efficiency and high time resolution," *APL Photonics* **6**(3), 036114 (2021).
79. F. Beutel et al., "Detector-integrated on-chip QKD receiver for GHz clock rates," *NPJ Quantum Inf.* **7**(1), 40 (2021).
80. B. Korzh et al., "Demonstration of sub-3 ps temporal resolution with a superconducting nanowire single-photon detector," *Nat. Photonics* **14**(4), 250–255 (2020).
81. A. S. Mueller et al., "Free-space coupled superconducting nanowire single-photon detector with low dark counts," *Optica* **8**(12), 1586–1587 (2021).
82. J. E. Bourassa et al., "Blueprint for a scalable photonic fault-tolerant quantum computer," *Quantum* **5**, 392 (2021).
83. J. M. Arrazola et al., "Quantum circuits with many photons on a programmable nanophotonic chip," *Nature* **591**(7848), 54–60 (2021).
84. L. S. Madsen et al., "Quantum computational advantage with a programmable photonic processor," *Nature* **606**(7912), 75–81 (2022).
85. L. You, "Superconducting nanowire single-photon detectors for quantum information," *Nanophotonics* **9**(9), 2673–2692 (2020).
86. E. Mykkänen et al., "Thermionic junction devices utilizing photon blocking," *Sci. Adv.* **6**(15), eaax9191 (2020).
87. A. Kemppinen et al., "Cascaded superconducting junction refrigerators: optimization and performance limits," *Appl. Phys. Lett.* **119**(5), 052603 (2021).
88. J. P. Höpker et al., "Integrated transition edge sensors on titanium in-diffused lithium niobate waveguides," *APL Photonics* **4**(5), 056103 (2019).
89. B. Calkins et al., "High quantum-efficiency photon-number-resolving detector for photonic on-chip information processing," *Opt. Express* **21**(19), 22657 (2013).
90. M. R. J. Palosaari et al., "Large 256-pixel X-ray transition-edge sensor arrays with Mo/TiW/Cu trilayers," *IEEE Trans. Appl. Supercond.* **25**(3), 1–4 (2015).
91. H. Akamatsu et al., "Demonstration of MHz frequency domain multiplexing readout of 37 transition edge sensors for high-resolution x-ray imaging spectrometers," *Appl. Phys. Lett.* **119**(18), 182601 (2021).
92. L. Grönberg et al., "Side-wall spacer passivated sub- μm Josephson junction fabrication process," *Supercond. Sci. Technol.* **30**(12), 125016 (2017).
93. J. Luomahaara et al., "Unshielded SQUID sensors for ultra-low-field magnetic resonance imaging," *IEEE Trans. Appl. Supercond.* **28**(4), 1–4 (2018).
94. S. Simbierowicz et al., "A flux-driven Josephson parametric amplifier for sub-GHz frequencies fabricated with side-wall passivated spacer junction technology," *Supercond. Sci. Technol.* **31**(10), 105001 (2018).
95. S. Simbierowicz et al., "Characterizing cryogenic amplifiers with a matched temperature-variable noise source," *Rev. Sci. Instrum.* **92**(3), 034708 (2021).
96. M. Perelshtein et al., "Broadband continuous variable entanglement generation using Kerr-free Josephson metamaterial," <https://arxiv.org/abs/2111.06145> (2021).
97. Single Quantum, "Application note: photon number resolving detectors," 2021, <https://singlequantum.com/wp-content/uploads/2021/09/ApplicationNotePNR.pdf>.
98. C. Cahall et al., "Multi-photon detection using a conventional superconducting nanowire single-photon detector," *Optica* **4**(12), 1534–1535 (2017).
99. R. Cheng et al., "A 100-pixel photon-number-resolving detector unveiling photon statistics," *Nat. Photonics* **17**(1), 112–119 (2023).
100. G. E. Hoefler et al., "Foundry development of system-on-chip InP-based photonic integrated circuits," *IEEE J. Sel. Top. Quantum Electron.* **25**(5), 1–17 (2019).
101. J. Lin et al., "Advances in on-chip photonic devices based on lithium niobate on insulator," *Photonics Res.* **8**(12), 1910–1936 (2020).
102. K. Luke et al., "Wafer-scale low-loss lithium niobate photonic integrated circuits," *Opt. Express* **28**(17), 24452–24458 (2020).
103. E. Obrzud et al., "Stable and compact RF-to-optical link using lithium niobate on insulator waveguides," *APL Photonics* **6**(12), 121303 (2021).
104. A. Prencipe, M. A. Baghban, and K. Gallo, "Tunable ultranarrowband grating filters in thin-film lithium niobate," *ACS Photonics* **8**(10), 2923–2930 (2021).
105. L. Chang et al., "CSOI: beyond silicon-on-insulator photonics," *Opt. Photonics News* **33**(1), 24–32 (2022).
106. T. Komljenovic et al., "Photonic integrated circuits using heterogeneous integration on silicon," *Proc. IEEE* **106**(12), 2246–2257 (2018).
107. M. Kapulainen et al., "Hybrid integration of InP lasers with SOI waveguides using thermocompression bonding," in *5th IEEE Int. Conf. Group IV Photonics*, pp. 61–63 (2008).
108. N. Somaschi et al., "Near-optimal single-photon sources in the solid state," *Nat. Photonics* **10**(5), 340–345 (2016).
109. E. Diamanti et al., "Practical challenges in quantum key distribution," *NPJ Quantum Inf.* **2**, npjq201625 (2016).
110. T. K. Paraíso et al., "A modulator-free quantum key distribution transmitter chip," *NPJ Quantum Inf.* **5**(1), 42 (2019).
111. C. Ma et al., "Silicon photonic transmitter for polarization-encoded quantum key distribution," *Optica* **3**(11), 1274–1278 (2016).

112. P. Sibson et al., “Chip-based quantum key distribution,” *Nat. Commun.* **8**(1), 1–6 (2017).
113. P. Sibson et al., “Integrated silicon photonics for high-speed quantum key distribution,” *Optica* **4**(2), 172–177 (2017).
114. H. Cai et al., “Silicon photonic transceiver circuit for high-speed polarization-based discrete variable quantum key distribution,” *Opt. Express* **25**(11), 12282–12294 (2017).
115. D. Bunandar et al., “Metropolitan quantum key distribution with silicon photonics,” *Phys. Rev. X* **8**(2), 021009 (2018).
116. G. Zhang et al., “An integrated silicon photonic chip platform for continuous-variable quantum key distribution,” *Nat. Photonics* **13**(12), 839–842 (2019).
117. M. Avesani et al., “Full daylight quantum-key-distribution at 1550 nm enabled by integrated silicon photonics,” *NPJ Quantum Inf.* **7**(1), 1–8 (2021).
118. T. K. Paraíso et al., “A photonic integrated quantum secure communication system,” *Nat. Photonics* **15**(11), 850–856 (2021).
119. L. Cao et al., “Chip-based measurement-device-independent quantum key distribution using integrated silicon photonic systems,” *Phys. Rev. Appl.* **14**(1), 011001 (2020).
120. M. Pittaluga et al., “600-km repeater-like quantum communications with dual-band stabilization,” *Nat. Photonics* **15**(7), 530–535 (2021).
121. S. Wang et al., “Twin-field quantum key distribution over 830-km fibre,” *Nat. Photonics* **16**(2), 154–161 (2022).
122. A. Boaron et al., “Secure quantum key distribution over 421 km of optical fiber,” *Phys. Rev. Lett.* **121**(19), 190502 (2018).
123. M. Lucamarini et al., “Overcoming the rate–distance limit of quantum key distribution without quantum repeaters,” *Nature* **557**(7705), 400–403 (2018).
124. D. Stucki et al., “Fast and simple one-way quantum key distribution,” *Appl. Phys. Lett.* **87**(19), 194108 (2005).
125. A. Boaron et al., “Simple 2.5 GHz time-bin quantum key distribution,” *Appl. Phys. Lett.* **112**(17), 171108 (2018).
126. L. C. Comandar et al., “Quantum key distribution without detector vulnerabilities using optically seeded lasers,” *Nat. Photonics* **10**(5), 312–315 (2016).
127. H.-L. Yin et al., “Measurement-device-independent quantum key distribution over a 404 km optical fiber,” *Phys. Rev. Lett.* **117**(19), 190501 (2016).
128. O. Kahl et al., “Spectrally multiplexed single-photon detection with hybrid superconducting nanophotonic circuits,” *Optica* **4**(5), 557–562 (2017).
129. X. Zheng et al., “Heterogeneously integrated, superconducting silicon-photonic platform for measurement-device-independent quantum key distribution,” *Adv. Photonics* **3**(5), 055002 (2021).
130. X. Chi et al., “Fractal superconducting nanowire single-photon detectors with reduced polarization sensitivity,” *Opt. Lett.* **43**(20), 5017–5020 (2018).
131. D. V. Reddy et al., “Broadband polarization insensitivity and high detection efficiency in high-fill-factor superconducting microwire single-photon detectors,” *APL Photonics* **7**(5), 051302 (2022).
132. C. Bruynsteen et al., “Integrated balanced homodyne photonic-electronic detector for beyond 20 GHz shot-noise-limited measurements,” *Optica* **8**(9), 1146–1152 (2021).
133. H. Forsten et al., “Millimeter-wave amplifier-based noise sources in SiGe BiCMOS technology,” *IEEE Trans. Microwaves Theory Tech.* **69**(11), 4689–4696 (2021).
134. M. Varonen et al., “Cryogenic W-band SiGe BiCMOS low-noise amplifier,” in *IEEEMTT- Int. Microwave Symp. IMS*, pp. 185–188 (2020).
135. S. Lischke et al., “Ultra-fast germanium photodiode with 3-dB bandwidth of 265 GHz,” *Nat. Photonics* **15**(12), 925–931 (2021).
136. K. C. Balram and K. Srinivasan, “Piezoelectric optomechanical approaches for efficient quantum microwave-to-optical signal transduction: the need for co-design,” *Adv. Quantum Technol.* **5**(3), 2100095 (2022).
137. J. Preskill, “Quantum computing in the NISQ era and beyond,” *Quantum* **2**, 79 (2018).
138. “A preview of Bristlecone, Google’s New Quantum Processor,” Google AI Blog, <https://ai.googleblog.com/2018/03/a-preview-of-bristlecone-googles-new.html>.
139. M. F. Gonzalez-Zalba et al., “Scaling silicon-based quantum computing using CMOS technology,” *Nat. Electron.* **4**(12), 872–884 (2021).
140. J. Duan et al., “Dispersive readout of reconfigurable ambipolar quantum dots in a silicon-on-insulator nanowire,” *Appl. Phys. Lett.* **118**(16), 164002 (2021).
141. S. Neyens, “High volume cryogenic measurement of silicon spin qubit devices from a 300 mm process line,” in *Silicon Quantum Electron. Workshop*, Orford (2022).
142. S. G. J. Philips et al., “Universal control of a six-qubit quantum processor in silicon,” *Nature* **609**(7929), 919–924 (2022).
143. H. Bohuslavskiy et al., “Scalable on-chip multiplexing of low-noise silicon electron and hole quantum dots,” <https://arxiv.org/abs/2208.12131> (2022).
144. D. S. Holmes, A. L. Ripple, and M. A. Manheimer, “Energy-efficient superconducting computing—power budgets and requirements,” *IEEE Trans. Appl. Supercond.* **23**(3), 1701610 (2013).
145. F. Lecocq et al., “Control and readout of a superconducting qubit using a photonic link,” *Nature* **591**(7851), 575–579 (2021).
146. B. Patra et al., “Cryo-CMOS circuits and systems for quantum computing applications,” *IEEE J. Solid-State Circuits* **53**(1), 309–321 (2018).
147. J. C. Bardin et al., “A 28 nm bulk-CMOS 4-to-8 GHz <2 mW cryogenic pulse modulator for scalable quantum computing,” in *IEEE Int. Solid-State Circuits Conf. (ISSCC)*, pp. 456–458 (2019).
148. X. Xue et al., “Quantum logic with spin qubits crossing the surface code threshold,” *Nature* **601**(7893), 343–347 (2022).
149. K. K. Likharev and V. K. Semenov, “RSFQ logic/memory family: a new Josephson-junction technology for sub-terahertz-clock-frequency digital systems,” *IEEE Trans. Appl. Supercond.* **1**(1), 3–28 (1991).
150. O. A. Mukhanov, “Energy-efficient single flux quantum technology,” *IEEE Trans. Appl. Supercond.* **21**(3), 760–769 (2011).
151. W. Chen et al., “Rapid single flux quantum T-flip flop operating up to 770 GHz,” *IEEE Trans. Appl. Supercond.* **9**(2), 3212–3215 (1999).
152. C. Lv et al., “Improving maximum count rate of superconducting nanowire single-photon detector with small active area using series attenuator,” *AIP Adv.* **8**(10), 105018 (2018).
153. A. J. Annunziata et al., “Reset dynamics and latching in niobium superconducting nanowire single-photon detectors,” *J. Appl. Phys.* **108**(8), 084507 (2010).
154. J. Münzberg et al., “Superconducting nanowire single-photon detector implemented in a 2D photonic crystal cavity,” *Optica* **5**(5), 658–665 (2018).
155. P. Ravindran et al., “Active quenching of superconducting nanowire single photon detectors,” *Opt. Express* **28**(3), 4099–4114 (2020).
156. S. Miki et al., “Photon detection at 1 ns time intervals using 16-element SNSPD array with SFQ multiplexer,” *Opt. Lett.* **46**(24), 6015–6018 (2021).
157. “Finland’s first 5-qubit quantum computer is now operational,” <https://www.vttresearch.com/en/news-and-ideas/finlands-first-5-qubit-quantum-computer-now-operational> (accessed 3 Jan. 2022).
158. V. Billault et al., “Free space optical communication receiver based on a spatial demultiplexer and a photonic integrated coherent combining circuit,” *Opt. Express* **29**(21), 33134–33143 (2021).
159. A. Gritsch et al., “Narrow optical transitions in erbium-implanted silicon waveguides,” *Phys. Rev. X* **12**(4), 041009 (2022).

Matteo Cherchi received his laurea degree in physics from the University of Pavia, Italy, in 1997, the certificate of advanced studies in mathematics from the University of Cambridge, UK, in 1998, and his Dottorato di Ricerca in electronic engineering from the University of Palermo, Italy, in 2008. He has been working on photonic integration research since 1999, both in industry and academia. In 2002, he acted as a visiting scientist at the Research Laboratory of Electronics of MIT, working closely with the groups of Prof. Hermann Haus and Prof. Lionel Kimerling. In 2011, he joined the Microphotonics Group of Prof. Michael R. Watts at MIT; he then moved to VTT's Silicon Photonics Team led by Dr. Timo Aalto. He is presently a principal scientist in the Quantum Photonics Team at VTT.

Arijit Bera received his MSc degree in photonics in 2013 and his PhD in silicon photonics in 2018 from the Institute of Photonics, University of Eastern Finland, Joensuu, Finland. He joined VTT in 2018 as a research scientist and has been working in the Silicon Photonics Team since 2020. He has gained expertise in PIC design and micro/nanofabrication of both active and passive photonic devices. His current research explores the interfaces of integrated photonics and the superconducting quantum technologies. Currently, he is in the Quantum Photonics Team at VTT.

Antti Kempainen received his MSc and DSc degrees in engineering physics and mathematics from Helsinki University of Technology in 2004 and 2009, respectively. He joined the Finnish National Metrology Institute in 2003, which was merged into VTT in 2015. Presently, he is a senior scientist in the Quantum Computing Hardware Team of VTT, where he coordinates European and national research projects. His research experience covers single-electron pumping, Josephson voltage standards, cryogenic thermometry, electrical refrigeration, superconducting nanowires, and cryogenic techniques, including their optical integration.

Jaani Nissilä received his MSc and doctoral degrees in engineering physics and mathematics from Helsinki University of Technology in 1994 and 2001, respectively. His studies focused on the development of instrumentation and methods for defect studies in semiconductors using positron annihilation techniques. In 2002, he joined the Finnish National Metrology Institute to develop quantum standards for electrical metrology, especially Josephson voltage standards and their applications. Since 2015, he has been developing optical methods for driving superconducting electronics with fast optical pulses and ultrafast photodiodes.

Kirsi Tappura received her MSc (Tech) (with distinction), LicSc (Tech), and DSc (Tech.) degrees in technical physics from the Tampere University of Technology (TUT, currently Tampere University, TAU), Finland, in 1990, 1992, and 1993, respectively, while focusing on semiconductor physics and optoelectronics including quantum structures. After a period in industry among innovative electronic display technologies, she joined VTT, where she has held various research and team leader positions and worked on a wide range of photonic/plasmonic, electronic, and thermal devices based on semiconductor, superconductor, and soft-matter systems, with an emphasis on computational physics. Since 1999, she has also been a docent of physics at TUT/TAU. She is currently a principal scientist in the Quantum Sensors Team at VTT.

Marco Caputo received his bachelor's and master's degrees in physics from the University of Salerno in 2013 and 2015, respectively, and his PhD in mathematics, physics, and applications from the University of Campania "Luigi Vanvitelli" in collaboration with the University of Salerno in 2018. During the time in academia, he studied the growth

and characterization of superconducting films for spintronics and optoelectronics applications. In 2020, he joined the Quantum Hardware and Quantum Sensors Teams at VTT as a research scientist focusing its activity on superconducting single-photon detectors. In 2022, he started working at Single Quantum as a research engineer.

Lauri Lehtimäki received his master's degree in theoretical physics from the University of Helsinki in 2018. After graduation, he worked in the field of photonic integration at VTT for 3 years. At VTT, he worked in the Silicon Photonics Team, led by Dr. Timo Aalto, where his work concentrated on designing optical circuits and components on the silicon-on-insulator platform. Presently, he is working for a startup where he develops data analysis and signal processing methods.

Janne Lehtinen was a research team leader of the Quantum Sensors Team at VTT during the manuscript writing and currently is a chief science officer of SemiQon Technologies Oy. He is an expert in semiconductor and superconducting device fabrication and characterization. He has been in leading roles in European and national projects and published more than 30 peer-reviewed publications.

Joonas Govenius earned his BA (*summa cum laude*) degree from Princeton University in 2010, his master's degree (with distinction) from ETH Zurich in 2012, and his doctoral degree from Aalto University in 2016, with a thesis on the design, fabrication, and characterization of an ultrasensitive microwave bolometer. In 2018, he joined VTT and, since 2020, he has been leading a research team of ~20 researchers focused on superconducting circuits, including qubits, sensors, and amplifiers.

Tomi Hassinen received his MSc and PhD degrees in physics from the University of Helsinki, Helsinki, Finland, in 2003 and 2018, respectively. He started working at VTT in 2006 and focused first on electronics production technologies. He is currently working as a senior scientist in the Silicon Photonics Team, doing research on component assembly and integration technologies. He has much experience in component characterization and conducts the team's high-speed component testing.

Mika Prunnila received his PhD from Aalto University in 2007 (Helsinki University of Technology at that time). He is a co-founder of SemiQon company. He is a professor in VTT's microelectronics and quantum technologies research area. His research has covered various aspects of micro/nano/quantum devices from physics to applications. He has authored/co-authored 80+ peer-reviewed journal papers and has patents/patent applications in ~17 patent families. He has been involved in preparation and execution of several collaborative national and international research projects. For example, currently he is coordinating a 21 partner Quantum Flagship project Qu-Pilot funded by the European Commission and a 12 partner Industrial Quantum Technology Ecosystem project QuTI funded by Business Finland.

Timo Aalto received his MSc and DSc (tech) degrees in optoelectronics technology from Helsinki University of Technology in 1998 and 2004, respectively, and has worked in silicon photonics research at VTT since 1997. He leads VTT's Silicon Photonics Research Team. His research focuses on the micron-scale silicon waveguides that are used to make ultracompact and low-loss photonic integrated circuits for communication, imaging, and sensing applications at infrared wavelengths. He has contributed to ~100 scientific publications, reviewed several EU projects, journal articles, and theses, and coordinated large projects funded by the EU, Business Finland, the European Space Agency, and industry.